Integrated Urinalysis Devices Based on Interface-Engineered Field Effect Transistor Biosensors Incorporated with Electronic Circuits

Yanbing Yang*, Jingfeng Wang, Wanting Huang, Guojia Wan, Miaomiao Xia, Duo Chen, Yun Zhang, Yiming Wang, Fuding Guo, Jie Tan, Huageng Liang, Bo Du, Lilei Yu*, Weihong Tan, Xiangfeng Duan, Quan Yuan*

Prof. Y. Yang, J. Wang, W. Huang, G. Wan, M. Xia, D. Chen, Y. Zhang, Y. Wang, F. Guo, Prof. B. Du, Prof. L. Yu, Prof. Q. Yuan

Department of Cardiology, Institute of Molecular Medicine, Renmin Hospital of Wuhan University, College of Chemistry and Molecular Sciences, School of Computer Science, Wuhan University, Wuhan, China.

E-mail: yuanquan@whu.edu.cn; yangyanbing@whu.edu.cn; lileiyu@whu.edu.cn

Dr. J. Tan, Prof. W. Tan, Prof. Q. Yuan

Molecular Science and Biomedicine Laboratory (MBL), State Key Laboratory of Chemo/Biosensing and Chemometrics, College of Chemistry and Chemical Engineering, Hunan University, Changsha, China.

Dr. H. Liang

Union Hospital, Tongji Medical College, Huazhong University of Science and Technology, Wuhan, China.

Prof. X. Duan

Department of Chemistry and Biochemistry, University of California Los Angeles, Los Angeles, CA, USA.

Abstract: Urinalysis is attractive in non-invasive early diagnosis of bladder cancer compared with clinical gold standard cystoscopy. However, the trace bladder tumor biomarkers in urine and the particularly complex urine environment pose significant challenges for urinalysis. Here, we report a clinically adoptable urinalysis device that integrates molecular-specificity indium gallium zinc oxide field-effect transistor (IGZO FET) biosensor arrays, a device control panel and an Internet terminal for directly analyzing 5 bladder tumor-associated proteins in clinical urine samples for bladder cancer diagnosis and classification. The IGZO FET biosensors with engineered sensing interfaces provide high sensitivity and selectivity for trace proteins identification in complex urine environment. Integrating with a machine-learning algorithm, our device could identify bladder cancer with an accuracy of 95.0% in a cohort of 197 patients and 75 non-BC individuals, distinguishing cancer stages with an overall accuracy of 90.0% and assessing bladder cancer recurrence after surgical treatment. The non-invasive urinalysis device defines a robust technology for remote healthcare and personalized medicine.

1. Introduction

Bladder cancer (BC) is one of the most common and aggressive malignant tumor in human urinary system with the increasing trend of morbidity and mortality worldwide. [1–4] The characteristics of complex pathologic patterns, the lack of obvious specific clinical symptoms, and high postoperative recurrence of BC requires more efficient diagnosis and prognosis of BC.[5,6] Current clinical gold standard cystoscopy for BC diagnosis relies on the insertion of an optical endoscope into the bladder cavity through urethra to image the suspected lesions.[7,8] This process is highly invasive and would cause urethra and bladder injury, resulting in hematuria and even urinary bacterial infection within a few days after examinations.[9] Critically, cystoscopy diagnosis is plagued with the inherent bladder tumor heterogeneity, and therefore limits the accuracy of early BC diagnosis.[10] Recently, noninvasive liquid biopsy is recently emerged as an alternative to address the bottleneck of

spatiotemporal tumor heterogeneity and to obtain disease-relevant molecular information for clinical cancer diagnosis and cancer status monitoring.[11–20]

Bladder is a urine storage organ that has been recognized as the metabolic microenvironment for bladder tumor cells, and its carcinogenesis and progression could make a pivotal impact on urine.[21] In this regard, the development of a urine biopsy provides a powerful strategy towards noninvasive early diagnosis and prognosis of BC. Clinically, urinalysis has been routinely utilized to detect abnormal metabolic biomarkers in urine for the assessment of health status and preliminary screening of diseases.[22–25] However, the physiologically relevant biomarkers detected by routine urinalysis are generally limited to high concentration targets over the micromolar level. On the other hand, the concentration of BC-relevant biomarkers in urine is usually extremely low, which is further complicated by the deeply complex urine environment. Hence, it is highly desirable to develop a clinical utility urinalysis technique with high sensitivity to identify trace bladder tumor biomarkers in urine for efficient early-stage and accurate BC diagnosis.

Here, we report and validate an integrated urinalysis device that is composed of an indium gallium zinc oxide field-effect transistor (IGZO FET) biosensor array, a device control unit and an Internet terminal to afford directly analysis of bladder tumor-associated proteins in untreated urine samples. In this urinalysis device, molecular-specificity IGZO FET sensing array units with engineered interfaces and high uniformity enable the simultaneous and reliable monitoring of five bladder tumor-associated protein molecules in urine samples, significantly improving the diagnostic accuracy. The device control panel with data conversion and wireless communication ability permit the real-time transmission of bladder tumor-associated protein signatures to the Internet terminal, which is further analyzed through machine learning algorithm. Overall, our technology delivers a 95.0% accuracy in identifying BC after analyzing the protein signatures in a cohort of urine samples from 197 BC patients and 75 non-BC individuals. Importantly, the integrated urinalysis device could distinguish among stage I-III cancer stages in BC patients with an accuracy of higher than 90.0% and is effective in monitoring the status of patients *in vivo* to enable the prognosis and guide the

therapy. This integrated urinalysis device performs the capability to real-time track the progression, metastatic and recurrence of BC as well as provides an efficient monitoring platform to promote the development of personalized health management.

2. Results and Discussion

2.1. Assay Validation

The IGZO FET devices were fabricated on a Si/SiO_2 substrate by photolithography in which Au source and drain electrodes were deposited by thermal evaporation, and the magnetic sputter-deposited IGZO layer with a thickness of 25 nm serves as channel material (Figure S1). The efficient biosensing relies firstly on the electrical performance of IGZO FET device. As indicated in Figure S2, the transfer characteristic of back-gated IGZO FET shows n-type transistor behavior with an on-state current of 40 μA, current on/off ratio of 1×10^6 and carrier mobility (μ_{FE}) of 15.8 cm^2 V^{-1} s^{-1}, and these electronic properties are comparable to that of previously reported works (Table S1).[26,27] Additionally, the transfer/output characteristics of IGZO FET device were well maintained under liquid-gated voltage, promising the extraordinary performance of IGZO FET in biosensing (Figure S3). To identify bladder tumor-relevant proteins in urine samples, a specific recognition molecule such as antibody should be functionalized on the IGZO FET device to achieve a biosensor (Figure 1a). In the biosensing process, the binding of charged target proteins with recognition molecules would induce the accumulation or depletion of carriers in the IGZO channel and generate a change in current amplitude (Figure 1b).

In biological buffer solutions, the charged protein molecules would be surrounded by oppositely charged ions due to electrostatic interaction, thus decreasing the effective charge of proteins.[28–41] This effect is known as Debye screening, and due to the Debye screening effect, the effective electrical field of FET biosensors could only be controlled within a distance called Debye length (λ_D):[42,43]

$$\lambda_D = \sqrt{\frac{\varepsilon k_B T}{2 N_A q^2 I}} \tag{1}$$

where ε is the dielectric constant of electrolyte. k_B, T and N_A represent the Boltzmann's constant, temperature and Avogadro's number, respectively. I is the ionic strength of the solution. q is the elementary charge. According to this equation, it is definite that λ_D is inversely proportional to ionic

strength, and the value of λ_D narrows from 7.0 nm to 0.7 nm when the concentration of phosphate-buffered saline (PBS) solution increases from 0.1 mM to 10 mM (Figure 1b).
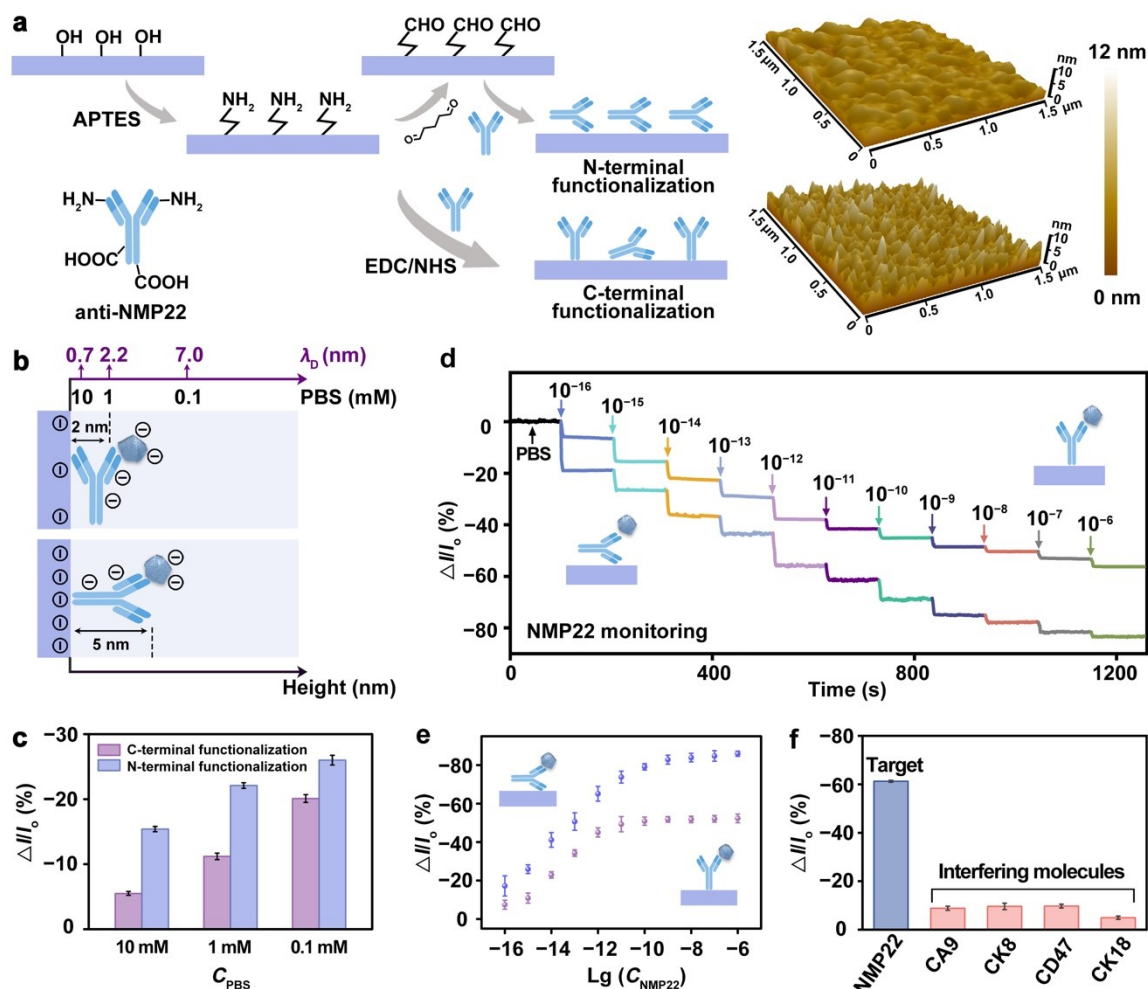

Figure 1. Interface engineering of FET biosensor. (a) Schematic and AFM images of anti-NMP22 functionalized on the IGZO device by N-terminal (top) and C-terminal (bottom). (b) Debye lengths of PBS buffer and protein height. The sensing mechanism of the IGZO FET biosensor was also plotted. (c) Current response of N-terminal and C-terminal functionalized anti-NMP22/IGZO FET biosensor towards NMP22 target under different ionic strengths. The concentration of NMP22 is 10^{-16} g mL^{-1}. (d) Real-time current response of N-terminal and C-terminal functionalized anti-NMP22/IGZO FET biosensor towards NMP22 with concentrations ranging from 10^{-16} to 10^{-6} g mL^{-1}. (e) Calibrated curves of N-terminal and C-terminal functionalized IGZO FET biosensors. The relationship between current response and logarithm of NMP22 concentration was plotted. The linear range of N-terminal and C-terminal functionalized anti-NMP22/IGZO biosensor is 10^{-16}-10^{-12} g mL^{-1} and 10^{-15}-10^{-12} g mL^{-1}, respectively. (f) Selectivity of N-terminal functionalized anti-NMP22/IGZO FET biosensor. The concentrations of target protein and interfering molecules are all 10^{-12} g mL^{-1}. All the error bars represent the standard deviations of three measurements.

In urine samples with extremely high ionic strength, the surface charge of proteins would be severely screened. To overcome this limitation, the arrangements of recognition molecules on the IGZO surface was regulated to minimize its occupied length for the purpose of narrowing the distance between target protein molecules and IGZO channel. Specifically, two different immobilization strategies that could bind different terminals of antibodies for bladder tumor-specific nuclear matrix protein 22 (anti-NMP22) were utilized to regulate antibody arrangements on IGZO (Figure 1a). The IGZO surface was firstly modified with (3-aminopropyl) triethoxysilane (APTES) to introduce amino groups. Subsequently, anti-NMP22 was separately immobilized on the IGZO surface by coupling to N-terminal with the assistance of glutaraldehyde or C-terminal through 1-ethyl-3-(3-dimethylaminopropyl) carbodiimide hydrochloride and N-hydroxysulfosuccinimide (EDC/NHS) chemistry. The presence of absorption peaks (1530 cm^{-1} and 1650 cm^{-1}) that were correspond to amide bonds in the attenuated total reflection flourier transformed infrared spectroscopy (ATR-FTIR) curves as well as the appearance of characteristic peaks for C 1s (286.6 eV), N 1s (399.9 eV), and S 2p (162.4 eV) in the X-ray photoelectron spectra (XPS) curves of N-terminal functionalized anti-NMP22/IGZO suggest that anti-NMP22 was successfully immobilized on the IGZO surface (Figure S4 and Figure S5). Since the pKa of amine groups at N-terminus is lower than 7.4 and the pKa of amine groups at side chains is higher than 7.4, a pH of 7.4 was used to ensure that the N-terminus of antibody is deprotonated and reactive to glutaraldehyde, while the side-chain amines are protonated and unable to react with glutaraldehyde. Consequently, the arrangement of antibodies on N-terminal functionalized IGZO biosensor is relatively uniform. By contrast, since the non-selective EDC/NHS chemistry would allow the conjugation of both C-terminus and side chain carboxyl groups, the arrangement of anti-NMP22 on C-terminal functionalized IGZO is relatively random. As confirmed by the increased surface roughness of C-terminal functionalized IGZO compared with that of N-terminal functionalization in the atomic force microscopy (AFM) images (Figure 1a). More importantly, the height of N-terminal and C-terminal functionalized anti-NMP22 measured with AFM are ~2-4 nm and ~5-7 nm (Figure S6 and Figure S7), and the average thickness of N-terminal and C-terminal functionalized antibody layer on the IGZO surface achieved by ellipsometer is about 3.3 nm and 5.8 nm. These results suggest that the regulation of antibody modification sites could control antibody orientations and the occupied length of antibody on IGZO.

To investigate the antibody orientation on the biosensing performance, the N-terminal and C-terminal functionalized IGZO biosensor towards NMP22 target with a concentration of 10^{-16} g mL^{-1} under different ionic strengths were investigated. The current response ($100 \times \Delta I/I_o$) that was

defined as the percentage change in I_d before and after NMP22 conjugation (ΔI) compared with I_o was recorded (Figure 1c). An optimized anti-NMP22 modification concentration and protein incubation time of 5 min were selected for the following measurements (Figure S8 and Figure S9). Figure 1c indicates that the N-terminal functionalized IGZO FET biosensor exhibits relatively high current responses across all the investigated PBS concentrations compared with that of C-terminal functionalization. At low ions strength of 0.1 mM PBS, the current response between N-terminal (26.0%) and C-terminal (20.0%) functionalized IGZO FET biosensor is relatively close, suggesting that the majority of charges on NMP22 target were located in the range of λ_D with a long distance of 7.0 nm. When the ionic strength increases to 1 mM and even 10 mM PBS, which corresponds to λ_D of 2.2 nm and 0.7 nm, the current response of N-terminal functionalized IGZO FET biosensor (22.1% and 15.7% at 1 mM and 10 mM PBS) is significantly higher than that of C-terminal functionalization (11.1% and 5.6% at 1 mM and 10 mM PBS). Based on the above results, it is recognized that the regulation of antibody orientation offers an efficient strategy to minimize the occupied length of antibodies and allows the target protein to be in closer proximity to IGZO (Figure 1b). This narrowed distance would enable more charges located in the range of λ_D and improve the current response.

Since the ionic strength of urine is equivalent to 10 mM PBS, we then selected 10 mM PBS to investigate the sensing performance of IGZO FET biosensor. As shown in Figure 1d and Figure S10, the real-time current response of IGZO FET biosensor maintains relatively stable during the whole monitoring process. Also, the anti-NMP22 functionalized IGZO (anti-NMP22/IGZO) FET biosensor conjugated by N-terminal exhibits relatively high current response towards NMP22 across all the investigated concentrations compared to that of C-terminal functionalization (Figure 1e and Figure S11). It is apparent that the anti-NMP22/IGZO FET biosensor exhibits an obvious current response of 17.2% upon the binding of NMP22 with a concentration of 10^{-16} g mL^{-1} and then exhibits a linear increase in current response as the concentration of NMP22 increases from 10^{-16} g mL^{-1} to 10^{-12} g mL^{-1}, which is boarder than that of C-terminal functionalized IGZO FET biosensor (10^{-15}-10^{-12} g mL^{-1}). The current variation is due to the accumulation of negative surface charge in n-type IGZO channel upon the binding of negatively charged NMP22. Additionally, the N-terminal and C-terminal functionalized anti-NMP22/IGZO FET biosensors all present a significantly high current response toward NMP22 target, while the current response for interfering molecules is relatively low (Figure 1f and Figure S12). The detection reproducibility was investigated by measuring the transfer characteristic curves of 8 anti-NMP22/IGZO FET biosensors after conjugation with NMP22 target (Figure S13). As shown in Figure S13, 8 transfer characteristic curves are highly consistent and the

calculated relative signal deviation (RSD) is 4.3%, demonstrating that the functionalized IGZO biosensors exhibit excellent detection stability. These results suggest the potential of IGZO biosensors for specific and reliable detection of bladder tumor-relevant proteins.

2.2. Clinical Investigations

To examine the applicability of IGZO FET biosensor for efficient bladder tumor-relevant proteins detection in urine environment, an IGZO FET biosensor array consisting of 5 detection channels capable of parallel measurements of a group of bladder tumor-relevant proteins, 3 control channels and 2 Ag/AgCl reference electrodes was designed (Figure 2a). A set of clinical-relevant bladder tumor urine biomarkers were tested for detection and validation: NMP22, membrane antigen carbonic anhydrase 9 (CA9), cluster of differentiation 47 (CD47), cytokeratin 8 (CK8) and cytokeratin 18 (CK18). The rationale for target protein selection was based on previous studies of expression difference in BC at different stages.[1,8] To enable selective detection, 5 types of antibody molecules that are specific to these bladder tumor-associated proteins were covalently functionalized on the IGZO FET biosensor array (Figure 2a and Figure S14). The real-time and calibrated current responses of CA9, CD47, CK8 and CK18 antibody molecules functionalized IGZO biosensors toward CA9, CD47, CK8 and CK18 exhibit similar response performance as that of anti-NMP22/IGZO FET biosensor (Figure S15-S19). The calculated detection limit (3 $\times$ standard deviation of the blank) of N-terminal functionalized IGZO biosensor array for NMP22, CA9, CD47, CK8 and CK18 is 3.2×10^{-17}, 6.2×10^{-18}, 3.7×10^{-17}, 1.6×10^{-18}, and 4.1×10^{-17} g mL^{-1}, which is about 10 folds lower than that of C-terminal functionalized IGZO FET biosensors (7.3×10^{-16}, 2.5×10^{-16}, 8.1×10^{-16}, 6.8×10^{-16}, and 2.1×10^{-15} g mL^{-1} for NMP22, CA9, CD47, CK8 and CK18), 10^3 folds lower than that of electrochemical assay (10^{-14} g mL^{-1} level), 10^9 folds lower than that of fluorescence assays (10^{-8} g mL^{-1} level) and extremely lower than that of previously reported IGZO FET biosensors (Table S2). The above results demonstrate that N-terminal functionalized IGZO biosensor array exhibits high sensitivity and could be used for rapid and facile identification of trace bladder tumor-associated proteins.

With excellent detection performance, the IGZO FET biosensor array was incubated with freshly collected urine samples for subsequent analysis. NMP22, CA9, CD47, CK8 and CK18 protein signatures were collected. Figure 2b and Figure S20 show that the IGZO FET biosensor array exhibits an obvious current variation upon exposing to BC patient urine samples, and the current response is significantly more obvious than that of healthy individuals. The intrinsic complexity of urine possibly would cause serious non-specific adsorption and decrease the detection sensitivity and accuracy.

Bovine serum albumin (BSA) was utilized to minimize non-specific adsorption and exclude weakly adsorbed biomolecules as validated by the increased current response after blocking (Figure 2c and Figure S21). Since conventional urinalysis approaches are not sufficiently sensitive to quantify the trace bladder tumor-relevant proteins in urine samples, the recovery measurement was performed to evaluate the detection accuracy of IGZO FET biosensor array. By adding a series concentration of target proteins into urine samples, the recovery of spiked proteins was investigated and listed in Table S3. The measured recovery ranges from 95.3% to 104.3%, indicating that our designed IGZO biosensor array is reliable for quantitative analysis of bladder tumor-associated proteins in clinical patient urine samples. To explore the detection reproducibility of the IGZO FET biosensor array, the current response of the biosensor towards the same BC patient urine sample was investigated. The response curves shown in Figure S22 for the same patient urine sample are highly consistent (RSD below 7.7%), which shows excellent reproducibility for patient urine samples analysis. The excellent reproducibility of the biosensor array is mainly attributed to the large-area uniform IGZO channel materials and antibody immobilization layer. Based on the above results, it is expected that the IGZO biosensor array would be a powerful tool for identifying bladder tumor-relevant proteins in human urine samples.

2.3. Clinical validation cohort

To enable clinical management diagnostics, following the pre-validation assays, we proceeded to patient-relevant testing with our IGZO FET biosensor array. We designed a training cohort with 100 patients (n = 100; 39 for stage I (T1), 34 for stage II (T2), and 27 for stage III (T3)) referred for clinically indicated BC diagnosed with image-guided aspiration and biopsy (Figure 2d, Table S4). All the patients gave informed consent for the clinical validations. Urine samples of 40 healthy individuals were selected for comparison. The expression levels of NMP22, CA9, CD47, CK8, and CK18 in urine that were calculated based on the calibrated response curves in Figure 1e and Figure S23 were summarized in Figure 2d, Figure 2e and Table S4. Each patient shows particularly different protein expression levels (10^{-16} to 10^{-11} g mL^{-1} level), suggesting the diversity of bladder tumor phenotypes. The statistical expression levels of 5 bladder tumor-associated proteins in BC patients are remarkably higher than in healthy individuals ($P < 0.005$), which is consistent with the upregulation expression theory of cancer.[44–46] Figure S23 also reveals upregulation of NMP22, CD47, CK18 and downregulation of CK8, CA9 as the increase of BC stages, which are in good agreement with previously reported works.[47]
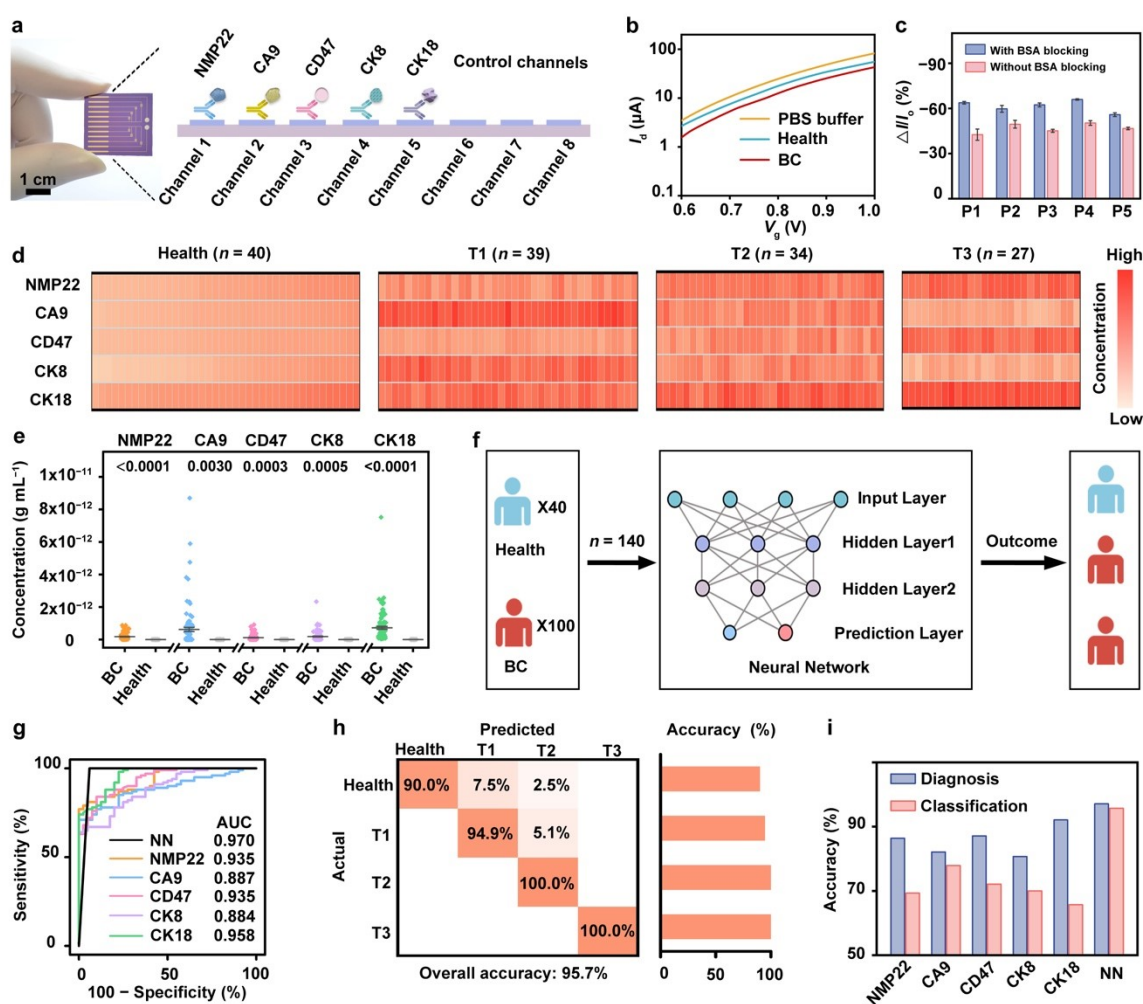
Figure 2. Clinical analysis of validation cohorts for BC diagnosis and classification. (a) Photograph and schematic of 8-channel sensing array, in which 5 channels are functionalized with specific antibody molecules for bladder tumor-relevant proteins, and the remaining 3 channels are utilized to record background signal of urine samples. (b) I_d-V_g curves of anti-NMP22/IGZO FET biosensor array in response to the urine samples from a BC patient and a healthy individual. (c) Current responses of anti-NMP22/FET biosensor array with and without BSA blocking for urine samples of 5 BC patients. P represents BC patients. No. 1-5 represent different patient samples. For example, "P1" represents a urine sample from BC patient No. 1. Error bars represent standard deviations of three measurements. (d) Heat map of 5 bladder tumor-relevant protein signatures in a training cohort. (n = 140; that is, 100 for untreated BC patients (including 39 cases in T1, 34 cases in T2 and 27 cases in T3) and 40 for healthy individuals. The color intensity indicates the concentration of protein. Among them, NMP22, CD47 and CK18 are up-regulated, CD47 and CK8 are down-regulated. (e) Comparison of expression levels of 5 bladder tumor-relevant proteins in urine samples from BC patients (n = 100) and healthy individuals (n = 40) (P < 0.005, unpaired two-sided t-test). (f) Schematic diagram of NN algorithm for the identification and classification of BC. The NN algorithm comprises four layers: an input layer, two fully connected hidden layers, and a prediction layer. (g) ROC curves showing high accuracy (AUC = 0.970) of NN algorithm in BC diagnosis, with its AUC significantly larger than that of

a single protein. (h) Confusion matrix summarizing the BC classification results in the training cohort. (i) Discrimination of BC patients from healthy individuals and classification of BC stages based on NN algorithm or a single protein.

The difference in expression levels of bladder tumor-associated proteins between BC patients and healthy individuals could potentially be used to give a discrimination. A machine learning algorithm neural network (NN) was exploited to analyze and train the 5 protein signatures obtained by IGZO FET biosensor array to make a decision (Figure 2f). For the analysis of urine samples with a single protein signature, a cut-off value that could maximize the detection sensitivity and specificity was exploited. The predicted results were compared with cystoscopy and tumor biopsies to determine the accuracy of our biosensor platform. The receiver operating characteristic (ROC) curves and precision-recall curves derived from NN algorithm and a single protein signature were constructed (Figure 2g and Figure S24). As indicated in Figure 2g, the area under the curve (AUC) of NN algorithm is significantly higher than those of individual protein signatures. The sensitivity and specificity for BC *versus* health differentiation predicted with NN algorithm reach 96.2% and 100%. In order to correlate antigen expression levels between BC stages and explore the capability of the biosensor for BC stages classification, the predicted and actual accuracy trained by NN algorithm with 5 protein signatures as inputs were mapped into a confusion matrix (Figure 2h). The NN algorithm generates a 94.9% accuracy for T1 BC identification, 100% accuracy for T2 BC identification and 100% accuracy for T3 BC identification. The overall diagnosis accuracy and classification accuracy achieved with NN algorithm is 97.1% and 95.7% (95% confidence interval (CI): 92.3%-99.1%). Notably, these values are significantly higher than those calculated with single protein signatures (Figure 2i and Figure S25). The above results validate that the simultaneous detection of 5 bladder tumor-relevant protein with IGZO FET biosensor array and the training of their combined protein signatures with NN algorithm are essential for effective BC diagnosis and classification.

2.4. Integrated urinalysis device for point-of-care diagnosis

An ultimate goal of our platform is to enable efficient point-of-care or home-care diagnosis for decentralized remote healthcare. In this regard, we integrated the IGZO FET biosensor array with micro-nano fabrication and wireless technology to achieve a portable device for urine analysis (Figure 3a-3c, Supplementary Video S1). The overall structure of the integrated urinalysis device mainly includes (1) an IGZO FET biosensor array for obtaining 5 bladder tumor-associated protein signatures from untreated urine samples; (2) a device control panel for acquiring detection data from the biosensor array and information communicating; (3) a smartphone and an application

program for data analysis and display (Figure 3b). The operation processes of the integrated urinalysis device are as follows: The microcontroller unit (MCU) in the data conversion module read instructions from the smartphone *via* a wireless Bluetooth unit and transfers the instructions to voltage signal through a digital-to-analog converter (DAC). Then, the voltage following module magnifies the voltage signal and apply voltage towards IGZO FET biosensor array. Subsequently, the MCU sequentially access the measured current signal from IGZO FET biosensor array and convert the signal into readable information by an 8-to-1 multiplexer (MUX), a trans-impedance amplifier (TIA) and an analog-to-digital converter (ADC). The Bluetooth unit export the readable information to a smartphone, and the application program that incorporates NN algorithm and diagnosis interface could analyze the received information to display the diagnosis results (Figure 3d). The urinalysis device was compatible with a power source to supply the whole device. The integrated urinalysis device is a portable device with an overall dimension of 15.2 cm (L) × 6.5 cm (W) × 2.4 cm (H), and it could be directly used for data acquisition, information communication and analysis (Figure 3c). Particularly, this stand-alone device could be easily operated by a variety of non-trained personnel and would not rely on well-instrumented laboratory or highly sophisticated analytical techniques. Specifically, after incubating 100 µL collected human urine directly on the device surface for 5 min, the integrated urinalysis device captures the bladder tumor-associated protein signatures simultaneously and analysis the detection data with the assistance of application program incorporated with NN algorithm automatically to display the diagnosis results (Figure 3e and 3f, Supplementary Video S2 and S3). Owing to the fast response speed of IGZO FET biosensor and the efficient detection signal transmission, the whole urinalysis process only requires less than 10 min. The diagnosis results displayed in Figure 3e and Figure 3f validate that the integrated urinalysis device could achieve efficient BC identification and classification. Notably, the component of urine is particularly complex and is influenced by human activities such as diet, rest, and movements, while the integrated urinalysis device with high stability and uniform biosensor array presents the ability to achieve parallel measurements of 5 protein signatures from urine samples. These features promise the potential of the integrated urinalysis device for clinical utility, point-of-care settings and health clinics in rural areas.
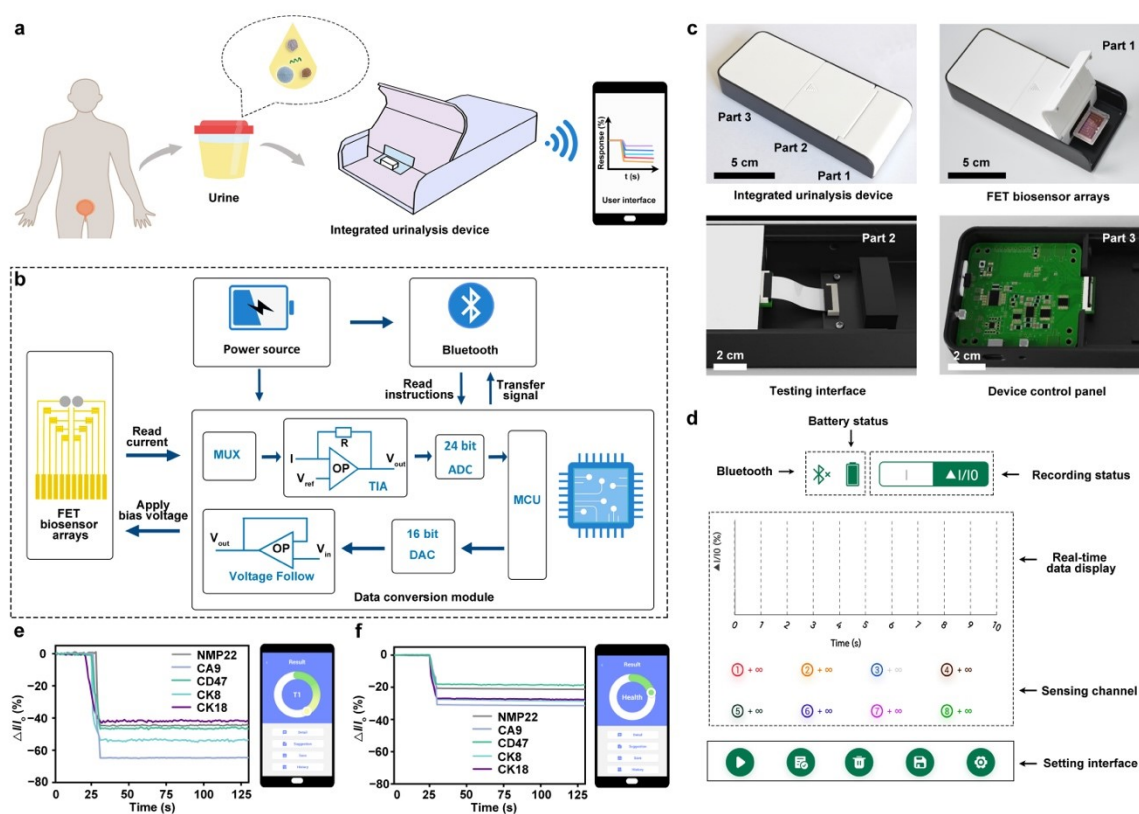
Figure 3. Integrated urinalysis device for point-of-care diagnosis. (a) Schematic of integrated urinalysis device for the detection of urine samples. (b) Circuit diagram and working principle of the integrated urinalysis device. c, Photograph of the integrated urinalysis device and the enlargement images of the three parts. (d) Testing interface and operation interface on the smartphone. (e-f) Current responses and diagnosis results of the integrated urinalysis device towards (e) a BC patient and (f) a healthy individual.

2.5. Double-blind prediction

To explore the clinical utility of the integrated urinalysis device, a testing cohort of patients (n = 65) with unknown diagnosis information and non-BC individuals (10 healthy individuals and 25 non-BC patients with urinary diseases) was selected for a blind prediction (Figure 4a and Table 1). The expression levels of bladder tumor-associated proteins summarized in Figure 4b and Figure S26 indicate that the BC patients show significantly high protein expression levels than non-BC patients and healthy individuals ($P < 0.005$). The prediction performance was evaluated with cystoscopy and tumor biopsies diagnosis results. As shown in Figure 4c, 4d and Table 1, a sensitivity of 100.0% and a specificity of 92.1% were achieved based on the ROC and precision-recall curves, and these values are significantly higher than that of estimated by urine cytology (sensitivity of 48.0% and specificity of 86.0%) and fluorescence in situ hybridization (FISH, 62.0% in sensitivity and 90.0% in

specificity).[47–49] These prediction results indicate that the integrated urinalysis device could enable effective BC diagnosis. For a further step, we explored the capability of the integrated urinalysis device for BC stages classification with the same testing cohort. As indicated in Figure 4e, the integrated urinalysis device could identify T1 BC with an accuracy of 84.2%, T2 BC with an accuracy of 87.5%, and T3 BC with an accuracy of 66.7%. The overall accuracy for BC diagnosis and classification with our established NN algorithm remain 95.0% and 90.0% (95% CI: 84.1%-95.9%), significantly higher than those calculated with single protein signatures (Figure S27). To further investigate the cancer stages classification capability of our integrated urinalysis device, we performed clinically applicable H&E histological analysis for selected BC patients. It is recognized that with the development of BC, the tumor cells would gradually invade the bladder wall and even surrounding tissues, and the nuclei of tumor cells would grow larger and irregular.[50] Based on these considerations, the BC stages were classified as shown in the H&E images in Figure 4f and Figure S28-30, and the classification results display good concordance with those obtained by urinalysis. The above analysis suggests that the integrated urinalysis device could be utilized in BC stages classification effectively. The reliable protein signatures identification capability and the high accuracy in BC diagnosis and classification possibly benefit from the high sensitivity, stability biosensor arrays and systematic database treatment with NN algorithm. These results highlight the ability of the integrated urinalysis device in identifying BC status, opening up the possibility to track the progression of BC.
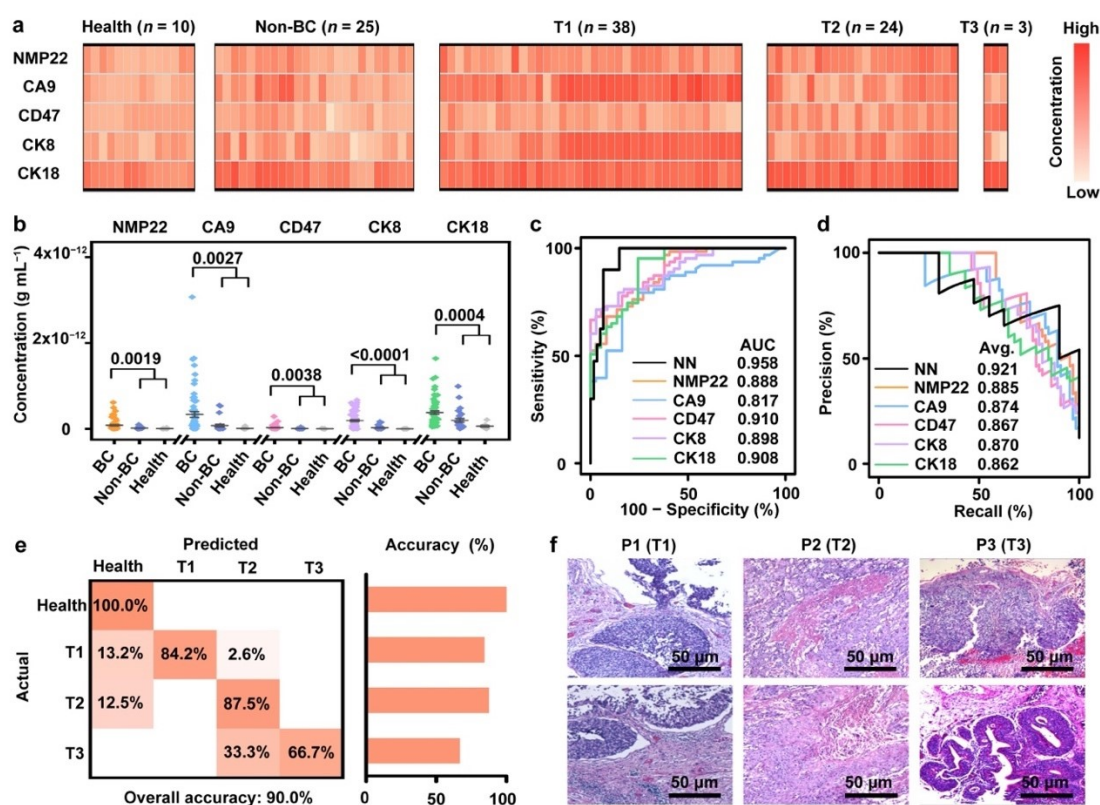
Figure 4. Blind prediction of testing cohorts for BC diagnosis and classification. (a) Application of the trained NN algorithm for the analysis of an independent testing cohort (*n* = 100; that is, 38 for T1, 24 for T2, 3 for T3, 25 for non-BC and 10 for healthy individuals). The concentrations of 5 proteins were shown by heat map. (b) Protein expression levels in urine samples from BC patients, non-BC patients and healthy individuals (*P* < 0.005, unpaired two-sided t-test). (c-d) ROC and precision-recall curves for the prediction of sensitivity and specificity in BC diagnosis based on NN algorithm and a single protein signature. The AUC of the NN algorithm is significantly higher than that of a single protein. (e) Confusion matrix summarizing the BC classification results in a testing cohort. (f) 6 representative tumor tissue images showing three BC patients at different stages.

Table 1. Summary of BC diagnostic statistics for single proteins and protein combination

Markers		Training cohort (*n* = 140)						Testing cohort (*n* = 100)			
		AUC	Avg. precision	Sensitivity (%)	Specificity (%)	Diagnosis accuracy (%)	Classification (%)	Sensitivity (%)	Specificity (%)	Diagnosis accuracy (%)	Classification (%)
Single proteins	NMP22	0.935	0.935	92.0	85.2	86.4	69.3	79.3	83.1	82.0	68.0
	CA9	0.887	0.922	69.2	87.1	82.1	77.9	83.3	85.7	85.0	63.0
	CD47	0.935	0.934	87.1	89.3	87.1	72.1	78.4	91.7	87.0	67.0

	CK8	0.884	0.918	84.1	67.9	80.7	70.0	81.8	79.5	79.0	65.0
	CK18	0.958	0.941	91.6	93.9	92.1	65.7	85.1	92.3	89.0	67.0
protein combination	NN	0.970	0.968	96.2	100.0	97.1	95.7	100.0	92.1	95.0	90.0
Clinical methods	Urinary cytology							48.0	86.0		
	FISH							62.0	90.0		

2.6. Longitudinal monitoring during clinical care

Longitudinal monitoring of protein signatures of BC patients could provide critical information regarding the progression of BC and enable effective prognosis. Especially, recording the real-time protein signatures offers the possibility to evaluate the cancer risk and provide the corresponding treatment strategy. Consequently, serial protein signatures of a cohort of patients (n = 16 for T1 patients and n = 16 for T2 patients) before and after surgery were tracked with the integrated urinalysis device (Figure 5a, Figure S31). Urine samples were collected 24 h before surgery and within one week after surgery. As shown in Figure 5a, the concentrations of proteins show an obvious decrease in all the patients, presumably due to the decreased proteins expression level in urine after curative tumor resection. To clearly present the change of protein signatures, the longitudinal protein signatures of NMP22, CA9, CD47, CK8 and CK18 were summarized in Figure 5b-5f for T1 BC patients (n = 16) and in Figure 5g-5k for T2 BC patients (n = 16). It can be clearly observed that all the investigated proteins show an obvious decrease, and this tendency is particularly notable for T2 patients (P < 0.05, paired t-test). Serial monitoring of bladder tumor-relevant protein signatures thus proposes a general strategy for cancer recurrence evaluation and prognosis tracking.
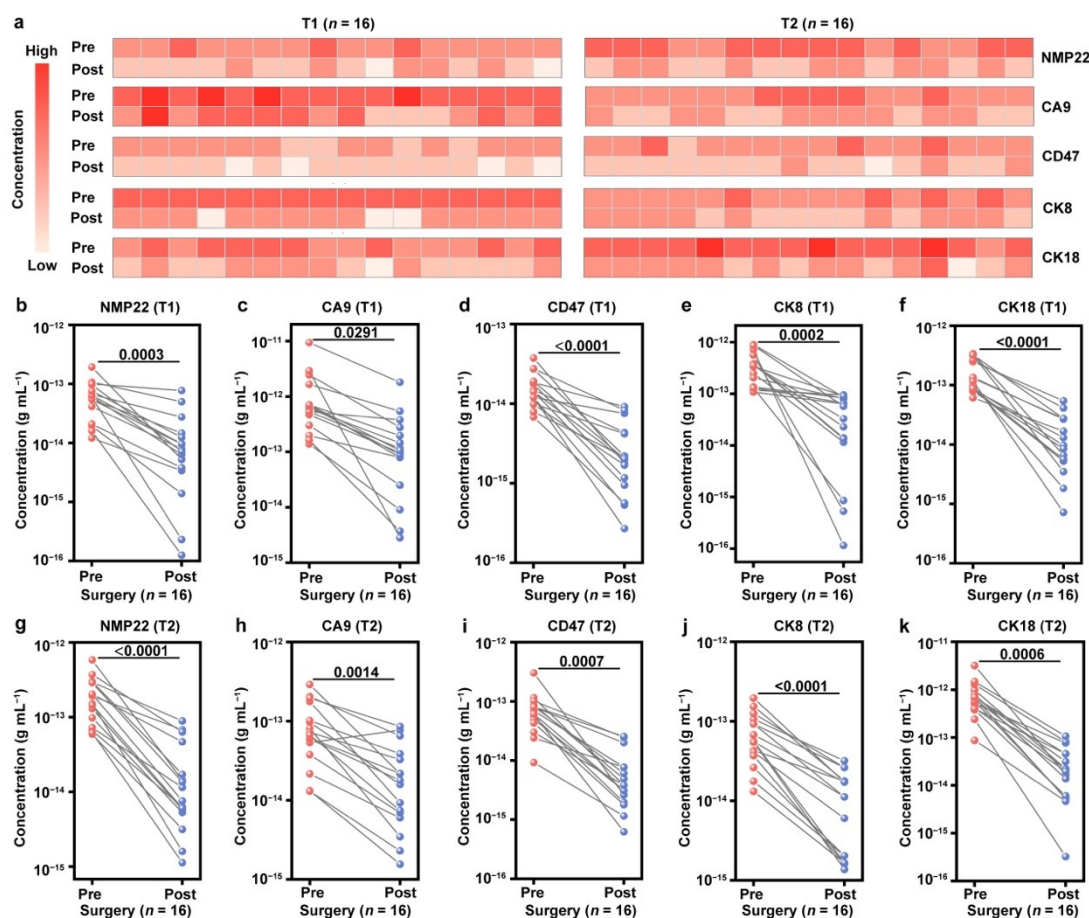
Figure 5. Longitudinal monitoring during clinical care. (a) Urine samples from BC patients (*n* = 32; 16 for T1 and 16 for T2) before and after surgery were analyzed by the integrated urinalysis device. The expression levels of 5 protein signatures were summarized by heat map. (b-k) Changes in the expression levels of 5 bladder tumor-relevant protein signatures from T1 and T2 BC patients before and after surgery ($P < 0.05$, paired two-sided t-test). (b) and (g) represent the changes of NMP22 level in urine samples from T1 and T2 BC patients before and after surgery, respectively. (c) and (h), (d) and (i), (e) and (j), (f) and (k) represent CA9, CD47, CK8 and CK18, respectively.

3. Conclusion

Overall, this work presents an integrated urinalysis device that is composed of an IGZO FET biosensor array, a device control panel and an Internet terminal to identify and analysis a group of bladder tumor-relevant proteins in urine samples for the achievement of clinical management. The interface of IGZO FET biosensor with excellent electrical performance was engineered to decrease the Debye screening effect originated from the high ionic strength of urine, thus enabling its capability for direct analysis of protein signatures in freshly collected urine samples. The urinalysis revealed that the bladder tumor-associated proteins in urine could reflect the critical signature of

BC, and the simultaneous detection and analysis of a panel of protein is necessary for efficient BC identification and cancer stages classification due to the intrinsic heterogeneous nature of tumor. Through the training of 5 protein signatures in urine samples from a cohort of 197 BC patients and 75 non-BC individuals, the integrated urinalysis device could achieve a 95.0% diagnosis accuracy and a 90.0% cancer stages classification accuracy. Also, the protein signatures show a significant correlation with treatment response. The serial monitoring of protein signature reflects that the protein expression levels decreased in all BC patients after surgical treatment, demonstrating the potential of the integrated urinalysis device for BC treatment monitoring, risk evaluation and prognosis. The integrated urinalysis device with the characteristics of portable, low-cost, non-invasiveness, automated data treatment and analysis that can be operated by non-trained personnel could potentially translate into standard clinical practice for cancer or critical diseases diagnostics and prognosis. A similar platform can be adapted for analysis of the other body fluids including blood and saliva for the point-of-care diagnosis of a wide range of biomarkers for personalized medicine.

4. Experimental Section/Methods

Materials and reagents:

Methanol, ethanol, isopropyl alcohol, acetone, glutaraldehyde (25.0%), Polyvinyl Butyral (PVB), iron(III) chloride ($FeCl_3$, > 99.0%) were purchased from Sinopharm Chemical Reagent Co., Ltd. EDC, NHS, Polymethyl methacrylate (PMMA) and APTES were obtained from Aladdin. BSA and PBS (0.1 mM, 1 mM and 10 mM, pH 7.4) were bought from Shanghai Yuanye Bio-Technology Co., Ltd. Bladder tumor-relevant proteins NMP22, CA9, CD47, CK8, CK18 and the corresponding antibody molecules anti-NMP22, anti-CA9, anti-CD47, ani-CK8, anti-CK18 were purchased from Dafeng Biotechnology Co., Ltd. The detailed information of these proteins was listed in Table S5.

Instrument and characterization:

The metallic electrodes (Cr/Au) array was patterned by ultra-violet (UV) lithography (ABM. Inc, America) and deposited by a thermal evaporator system (Jiashuo JSD-300, China). The IGZO channel layer was deposited by a radio frequency sputtering system with the assistance of mask templates (Jiashuo JSD300-Ⅱ China). The sensing area of the FET biosensor was exposed by an electron beam lithography system (EBL, JSM-6510, Japan). The microscopy images of the IGZO sensing electrodes

were obtained by an optical microscope (Olympus BX53MRF-S). The immobilization of antibody molecules on the IGZO surface was characterized by XPS (ESCAI AB250Xi, USA) and ATR-FTIR (FTIR5700, USA). The surface morphology and thickness of IGZO layer were characterized by AFM (Park nx10, Korea), ellipsometer (J.A. Woollam M-2000®, USA) and high-resolution field emission SEM (FEI Verios 460, USA). The ellipsometer characterization was performed at wavelength between 300 nm and 1000 nm at the incident angle of 65°, 70°, and 75°. The functionalized thickness of anti-NMP22 on the device was fitted by the Cauchy model. The electrical characteristics of the IGZO FET device were measured by a digital source meter (Agilent B2902A, USA) connected to a probe station.

Clinical samples:

Urine samples of BC patients were provided by Union Hospital of Wuhan and Renmin Hospital of Wuhan University. Urine samples of healthy individuals and non-BC patients were collected from Wuhan University and Renmin Hospital of Wuhan University. All relevant ethical laws and regulations concerning human participants were complied with. The study was approved by the Ethics Committee of Union Hospital of Wuhan and Renmin Hospital of Wuhan University. All the participants in this study signed informed consent forms before participating. In this study, the gender, age and pathological diagnosis results of all clinical samples were recorded anonymously.

H&E histological analysis:

Histological analysis of bladder tumor tissues was performed by paraffin-embedded tissue sections fixed with 10% formalin. The bladder tumor tissue samples were sectioned at a thickness of 5 um and stained with hematoxylin and eosin (H&E) for imaging. The images were obtained with an Olympus CKX53 inverted microscope slide scanner at 100 × magnification.

Fabrication of IGZO FET array:

The IGZO FET array was fabricated by the following processes. First, the interdigital source, drain and gate electrodes (15 nm Cr/50 nm Au) were deposited with thermal evaporation after patterned by photolithography. The channel length and width were 480 μm and 500 μm, respectively. Then, the

IGZO channel layer was deposited between patterned source and drain electrodes by magnetron sputtering with the assistance of a mask template. Ag/AgCl reference electrodes were fabricated by sequentially dip-coating silver colloid on the gate electrode, heating at 75 $^{\circ}$C for 15 min to evaporate solvent, dropping 0.1 M $FeCl_3$ solution on the silver colloid and reacting for 4 min to form AgCl layer. The surface of AgCl electrode was then treated with PVB-methanol solution for 3 h at room temperature to form a protective layer.

IGZO FET electrical characteristics evaluation:

The μ_{FE} and transconductance (g_m) of IGZO device was calculated based on the transfer characteristic curves in Figure S2. Since the interdigital electrode is composed of four independent electrodes in parallel, the μ_{FE} of IGZO device is 1/4 of the apparent and it can be calculated by:

$$\mu_{FE} = \frac{g_m L}{4WV_d C_{ox}} = \frac{dI_d L}{dV_g 4WV_d C_{ox}} \tag{2}$$

where L and W represent the channel length (480 μm) and width (500 μm). C_{ox} is 11.5 nF/cm^2 for Si wafer with 300 nm SiO_2 dielectric layer. V_d is set at 0.2 V. Based on equation (2), it is calculated that the μ_{FE} of IGZO device is 15. 8 cm^2 V^{-1} s^{-1}. The obtained maximized value of g_m calculated by I_d-V_g curve is 1.0 μS.

Fabrication of IGZO FET biosensor array:

To achieve selectively functionalization of antibody molecules on the IGZO sensing channel and avoid gate leakage current, the IGZO FET array was spin-coated with a layer of PMMA as protection layer and the IGZO sensing region with an area of 480 × 500 μm^2 was exposed by electron beam lithography. The device was then integrated with a PDMS well (with 2.5 cm length, 1.5 cm width and 0.3 cm height) for selectively functionalization and sensing. Subsequently, the IGZO layer was covalently functionalized with APTES to introduce amine groups on the IGZO. Specifically, 1 mL of 5% APTES in ethanol was dropped into the PDMS chamber for 1 h, and then heated in an oven at 110 $^{\circ}$C for 30 minutes to strengthen the silanization of APTES.[51] Then, 1 mL glutaraldehyde (5%) PBS buffer solution was added into the chamber and reacted for 2 h at room temperature to serve as linker molecules for conjugating N-terminal antibody molecules. To obtain N-terminal functionalized IGZO

FET biosensor, 100 μL antibody solution was added onto the IGZO channel and coupled with glutaraldehyde for 12 h at 4 $^\circ$C.[52] After BSA (0.01 g mL^{-1}) blocking at 4 $^\circ$C for 12 h and PBS buffer washing, N-terminal functionalized IGZO FET biosensor was obtained. C-terminal functionalized IGZO FET biosensor was prepared by sequentially adding 4 mL of EDC/NHS PBS solution (containing 20 μg EDC and 10 μg NHS) and 100 μL antibody solution onto the surface of APTES functionalized IGZO FET array, and shaking at room temperature for 2 h to couple with C-terminal antibody. It is worth noting that the 8-channel sensing array is consists of 5 detection channels for parallel measurements and 3 control channels for background signal recording. The control channels were obtained by blocking glutaraldehyde coupled IGZO with BSA to minimize urine environment such as ions strength and pH on the influence of sensing performance. To explore the optimized antibody functionalization concentration, a series of antibody solution with concentrations ranging from 10-30 μg mL^{-1} was investigated (Figure S8). Based on the measured current response, it is determined that the optimized concentration for anti-NMP22, anti-CA9, anti-CD47, anti-CK8 and anti-CK18 is 20 μg mL^{-1}.

Detection of bladder tumor-relevant proteins:

Before the measurements, the target protein incubation time was determined as 5 min to achieve the optimized current response (Figure S9). To investigate the relationship between ionic strength of PBS buffer and current response of biosensor, the current response of anti-NMP22/IGZO FET biosensor towards NMP22 target (10^{-16} g mL^{-1}) was recorded under different concentrations of PBS buffer (0.1 mM-10 mM). The real-time current response (I_d-t curves) of molecular specificity IGZO FET biosensor array was measured by successively injecting 100 μL target protein solution with a range of concentrations (10^{-16}-10^{-6} g mL^{-1}) into the PDMS chamber. The calibrated response curves were recorded by measuring the current response of the IGZO FET biosensor array before and after target proteins conjugation. The I_d-V_g curves were recorded at V_d = 0.2 V. The I_d-t curves were recorded at V_d = 0.2 V and V_g = 0.6 V. The selectivity of the IGZO FET biosensor array was evaluated by monitoring each antibody molecule functionalized IGZO FET biosensor unit towards the target protein and interfering molecules. For example, for NMP22 specific IGZO FET biosensor, NMP22 was used as the target, and CA9, CD47, CK8 and CK18 were selected as interfering molecules. The concentrations of the target and interfering molecules are all 10^{-12} g mL^{-1}. The recovery measurements were performed by adding a series concentration of target proteins into the urine samples and calculating the found target proteins concentration.

Construction of integrated urinalysis device:

The portable urinalysis device was integrated by an IGZO FET biosensor array, a Li-ion battery, a Bluetooth unit, a multiplexer (MUX), a trans-impedance amplifier (TIA), an analogue-to-digital converter (ADC), a digital-to-analogue converter (DAC), a voltage following module, and a microcontroller (MCU) unit. The NN algorithm was input into the smartphone to realize the analysis of the received data. We also developed an application program that includes operation interfaces, testing interfaces and diagnosis results interfaces for real-time data presentation and analysis. The diagnosis results could be presented on the interface to provide clinical suggestions and the corresponding diagnosis data could be saved in the smartphone.

Clinical urine samples analysis:

For clinical urine samples real-time detection, the integrated urinalysis device was firstly exposed to PBS electrolyte to record the initial current value I_o and then recorded the specific current signal after adding 100 µL urine samples into the PBS electrolyte. The urine incubation time was remained for 5 min. The average current signal was generated by recording the current responses of the device towards a specific urine sample for 60 s. A training cohort of 100 BC patients and 40 healthy individuals as well as a testing cohort of 65 BC patients, 25 non-BC patients and 10 healthy individuals were used for evaluation. The protein concentration was calculated based on the linear range in the calibrated response curves in Figure 1e and Figure S16. The obtained protein signatures were used for subsequent machine learning analysis.

Machine learning for BC diagnosis and classification:

NN model for BC diagnosis and classification was used in this study. Specifically, we set each biomarker value as an input feature x_i. Let a feature vector $\boldsymbol{x} = [x_1, x_2, \cdots, x_n]$ denote n biomarker values. To deal with the numerical instability problem that the original marker values are too low ($< 10^{-9}$), we standardized features by removing the mean and scaling to unit variance,

$$x' = \frac{x - \mu}{\sigma} \tag{3}$$

where μ denotes the mean of the training sample, σ is the standard deviation of the training samples.

Then we use Multi-layer Perceptron (MLP) to learn a classifier for cancer classification,

$$x_{h+1} = \varphi(x_h \cdot W + b) \tag{4}$$

where x_h is the input vector for h-th linear layer. W is the weights, and b is the bias. In our experiments, the dimension of hidden layers is optimized and fixed as 100. The layer number is 3. φ is the ReLU activation function.

In the last layer, we use a softmax classifier to predict,

$$c = \arg\max_i \frac{\exp(\dot{x})}{\sum_K \exp(\dot{x}_\iota)} \tag{5}$$

where $\dot{x}$ denotes the output vector of the last layer. $K = 4$ is the number of types, including $\{Health, T_1, T_2, T_3\}$. c is the predicting class. The hyperparameters of the neural network were optimized by the adaptive stochastic gradient descent method.[53]

The detailed analysis processes are as follows. The whole samples collected in this paper were randomly split into the training set (60%) and the blind testing set (40%). The diagnostic efficiency of the algorithm was evaluated based on the concentrations of five protein signatures fed into the output of the NN algorithm. The AUC values of ROC curves, Accuracy, Recall, and Precision were reported for evaluating our models. Our models were implemented with an open-source machine learning toolkit, Scikit-Learn, in the platform of Python 3.8.1, Ubuntu Linux 16.04 LTS.[54] The hardware environment is with Intel Xeon® CPU E5-2620, NVIDIA TITAN Xp*3. In order to deploy our classification model in portable mobile devices, we exported the weights trained by our model and refactored the model with C++ environment.

Statistical analysis:

The sensing current response of clinical samples was obtained from 5 parallel tests, and expression levels of bladder tumor-relevant proteins were organized in the heat maps via Origin 2022 (https://www.originlab.com/). The significance between expression levels of 5 bladder tumor-relevant proteins in urine samples from BC patients and healthy individuals was tested using an unpaired two-sided t-test. The significance between expression levels of 5 bladder tumor-relevant protein signatures before and after surgery was tested using a paired two-sided t-test. Statistical significance of the data was calculated at 95% ($P < 0.05$) CIs. ROC and precision-recall curves were constructed to evaluate the accuracy of bladder cancer diagnosis and classification. Sensitivity was defined as the probability that a test result was positive when cancer was detected (true positive rate), specificity as the probability that a test result was negative when cancer was not detected (true negative rate), and accuracy as the overall probability that an individual was correctly classified. The 95% CIs were calculated using a binomial distribution. Significance analyses, construction of ROC and precision-recall curves, and AUC calculation were performed using GraphPad Prism 8 (https://www.graphpad.com/scientific-software/prism/).

Supporting Information

Supporting Information is available from the Wiley Online Library or from the author.

References

[1] A. M. Kamat, N. M. Hahn, J. A. Efstathiou, S. P. Lerner, P.-U. Malmström, W. Choi, C. C. Guo, Y. Lotan, W. Kassouf, Bladder Cancer. *The Lancet* **2020**, *388*, 2796.

[2] S. Antoni, J. Ferlay, I. Soerjomataram, A. Znaor, A. Jemal, F. Bray, Bladder Cancer Incidence and Mortality: A Global Overview and Recent Trends. *Eur. Urol.* **2017**, *71*, 96.

[3] A. G. Robertson, J. Kim, H. Al-Ahmadie, J. Bellmunt, G. Guo, A. D. Cherniack, T. Hinoue, P. W. Laird, K. A. Hoadley, R. Akbani, M. A. A. Castro, E. A. Gibb, R. S. Kanchi, D. A. Gordenin, S. A. Shukla, F. Sanchez-Vega, D. E. Hansel, B. A. Czerniak, V. E. Reuter, X. Su, B. de Sa Carvalho, V. S. Chagas, K. L. Mungall, S. Sadeghi, C. S. Pedamallu, Y. Lu, L. J. Klimczak, J. Zhang, C. Choo, A. I. Ojesina, S. Bullman, K. M. Leraas, T. M. Lichtenberg, C. J. Wu, N. Schultz, G. Getz, M. Meyerson, G. B. Mills, D. J. McConkey, T. R. Network, J. N. Weinstein, D. J. Kwiatkowski, S. P. Lerner, Comprehensive Molecular Characterization of Muscle-Invasive Bladder Cancer. *Cell* **2017**, *171*, 540.

[4] X. Wei, F. Bian, X. Cai, Y. Wang, L. Cai, J. Yang, Y. Zhu, Y. Zhao, Multiplexed Detection Strategy for Bladder Cancer MicroRNAs Based on Photonic Crystal Barcodes. *Anal. Chem.* **2020**, *92*, 6121.

[5] E. J. Kouba, L. Cheng, Understanding the Genetic Landscape of Small Cell Carcinoma of the Urinary Bladder and Implications for Diagnosis, Prognosis, and Treatment: A Review. *JAMA Oncol.* **2017**, *3*, 1570.

[6] C. Pettenati, M. A. Ingersoll, Mechanisms of BCG Immunotherapy and Its Outlook for Bladder Cancer. *Nat. Rev. Urol.* **2018**, *15*, 615.

[7] T. Powles, J. P. Eder, G. D. Fine, F. S. Braiteh, Y. Loriot, C. Cruz, J. Bellmunt, H. A. Burris, D. P. Petrylak, S.-l. Teng, X. Shen, Z. Boyd, P. S. Hegde, D. S. Chen, N. J. Vogelzang, MPDL3280A (anti-PD-L1) Treatment Leads to Clinical Activity in Metastatic Bladder Cancer. *Nature* **2014**, *515*, 558.

[8] A. M. Kamat, P. K. Hegarty, J. R. Gee, P. E. Clark, R. S. Svatek, N. Hegarty, S. F. Shariat, E. Xylinas, B. J. Schmitz-Drager, Y. Lotan, L. C. Jenkins, M. Droller, B. W. van Rhijn, P. I. Karakiewicz, International Consultation on Urologic Disease-European Association of Urology Consultation on Bladder, C. ICUD-EAU International Consultation on Bladder Cancer 2012: Screening, Diagnosis, and Molecular Markers. *Eur. Urol.* **2013**, *63*, 4.

[9] H. M. Huang, H. X. Li, Tumor Heterogeneity and the Potential Role of Liquid Biopsy in Bladder Cancer. *Cancer Commn.* **2021**, *41*, 91.

[10] F. Descotes, N. Kara, M. Decaussin-Petrucci, E. Piaton, F. Geiguer, C. Rodrigurz-Lafrasse, J. E. Terrier, J. Lopez, A. Ruffion, Non-Invasive Prediction of Recurrence in Bladder Cancer by Detecting Somatic TERT Promoter Mutations in Urine. *Br. J. Cancer* **2017**, *117*, 583.

[11] C. Liu, J. Zhao, F. Tian, L. Cai, W. Zhang, Q. Feng, J. Chang, F. Wan, Y. Yang, B. Dai, Y. Cong, B. Ding, J. Sun, W. Tan, Low-Cost Thermophoretic Profiling of Extracellular-Vesicle Surface Proteins for the Early Detection and Classification of Cancers. *Nat. Biomed. Eng.* **2019**, *3*, 183.

[12] J. Deng, F. Tian, C. Liu, Y. Liu, S. Zhao, T. Fu, J. Sun, W. Tan, Rapid One-Step Detection of Viral Particles Using an Aptamer-Based Thermophoretic Assay. *J. Am. Chem. Soc.* **2021**, *143*, 7261.

[13] J. Zhou, Z. Wu, J. Hu, D. Yang, X. Chen, Q. Wang, J. Liu, M. Dou, W. Peng, Y. Wu, W. Wang, C. Xie, M. Wang, Y. Song, H. Zeng, C. Bai, High-Throughput Single-EV Liquid Biopsy: Rapid, Simultaneous, and Multiplexed Detection of Nucleic Acids, Proteins, and Their Combinations. *Sci. Adv.* **2020**, *6*, eabc1204.

[14] G. Siravegna, S. Marsoni, S. Siena, A. Bardelli, Integrating Liquid Biopsies into the Management of Cancer. *Nat. Rev. Clin. Oncol.* **2017**, *14*, 531.

[15] C. L. Ji, J. Tan, Q. Yuan, Defect Luminescence Based Persistent Phosphors-From Controlled Synthesis to Bioapplications. *Chinese J. Chem.* **2021**, *39*, 3188.

[16] Y. M. D. Lo, D. S. C. Han, P. Jiang, R. W. K. Chiu, Epigenetics, Fragmentomics, and Topology of Cell-Free DNA in Liquid Biopsies. *Science* **2021**, *372*, eaaw3616.

[17] Q. Zhou, J. Pan, S. Deng, F. Xia, T. Kim, Triboelectric Nanogenerator-Based Sensor Systems for Chemical or Biological Detection. *Adv. Mater.* **2021**, *33*, e2008276.

[18] M. Ratner, Jury out on Liquid Biopsies for Cancer. *Nat. Biotechnol.* **2018**, *36*, 209.

[19] L. Cai, S. Zhang, J. Miao, Z. Yu, C. Wang, Fully Printed Stretchable Thin-Film Transistors and Integrated Logic Circuits. *ACS Nano* **2016**, *10*, 11459.

[20] A. Clifford, J. Das, H. Yousefi, A. Mahmud, J. B. Chen, S. O. Kelley, Strategies for Biomolecular Analysis and Continuous Physiological Monitoring. *J. Am. Chem. Soc.* **2021**, *143*, 5281.

[21] A. R. J. Lawson, F. Abascal, T. H. H. Coorens, Y. Hooks, L. O'Neill, C. Latimer, K. Raine, M. A. Sanders, A. Y. Warren, K. T. A. Mahbubani, B. Bareham, T. M. Butler, L. M. R. Harvey, A. Cagan, A. Menzies, L. Moore, A. J. Colquhoun, W. Turner, B. Thomas, V. Gnanapragasam, N. Williams, D. M. Rassl, H. Vöhringer, S. Zumalave, J. Nangalia, J. M. C. Tubío, M. Gerstung, K. Saeb-Parsy, M. R. Stratton, P. J. Campbell, T. J. Mitchell, I. Martincorena, Extensive Heterogeneity in Somatic Mutation and Selection in the Human Bladder. *Science* **2020**, *370*, 75.

[22] J. Kaiser, 'Liquid Biopsy' for Cancer Promises Early Detection. *Science* **2018**, *359*, 259.

[23] Z. Ou, K. Li, T. Yang, Y. Dai, M. Chandra, J. Ning, Y. Wang, R. Xu, T. Gao, Y. Xie, Q. He, Y. Li, Q Lu, L. Wang, Z. Song, Detection of Bladder Cancer Using Urinary Cell-Free DNA and Cellular DNA. *Clin. Transl. Med.* **2020**, *9*, 4.

[24] S. M. Park, D. D. Won, B. J. Lee, D. Escobedo, A. Esteva, A. Aalipour, T. J. Ge, J. H. Kim, S. Suh, E. H. Choi, A. X. Lozano, C. Yao, S. Bodapati, F. B. Achterberg, J. Kim, H. Park, Y. Choi, W. J. Kim, J. H. Yu, A. M. Bhatt, J. K. Lee, R. Spitler, S. X. Wang, S. S. Gambhir, A Mountable Toilet System for Personalized Health Monitoring via the Analysis of Excreta. *Nat. Biomed. Eng.* **2020**, *4*, 624.

[25] Y. Yu, H. Jin, D. Holder, J. S. Ozer, S. Villarreal, P. Shughrue, S. Shi, D. J. Figueroa, H. Clouse, M. Su, N. Muniappa, S. P. Troth, W. Bailey, J. Seng, A. G. Aslamkhan, D. Thudium, F. D. Sistare, D. L. Gerhold, Urinary

Biomarkers Trefoil Factor 3 and Albumin Enable Early Detection of Kidney Tubular Injury. *Nat. Biotechnol.* **2010**, *28*, 470.

[26] Y. Q. Liang, M. M. Xiao, D. Wu, Y. X. Lin, L. J. Liu, J. P. He, G. J. Zhang, L. M. Peng, Z. Y. Zhang, Wafer-Scale Uniform Carbon Nanotube Transistors for Ultrasensitive and Label-Free Detection of Disease Biomarkers. *ACS Nano* **2020**, *14*, 8866.

[27] J. X. Liu, X. H. Chen, Q. Q. Wang, M. M. Xiao, D. L. Zhong, W. Sun, G. Y. Zhang, Z. Y. Zhang, Ultrasensitive Monolayer MoS2 Field-Effect Transistor Based DNA Sensors for Screening of Down Syndrome. *Nano Lett.* **2019**, *19*, 1437.

[28] Y. Yang, X. Yang, X. Zou, S. Wu, D. Wan, A. Cao, L. Liao, Q. Yuan, X. Duan, Ultrafine Graphene Nanomesh with Large On/Off Ratio for High-Performance Flexible Biosensors. *Adv. Funct. Mater.* **2017**, *27*, 1604096.

[29] Y. Liu, X. Duan, H. J. Shin, S. Park, Y. Huang, X. Duan, Promises and Prospects of Two-Dimensional Transistors. *Nature* **2021**, *591*, 43.

[30] J. Y. Oh, S. Rondeau-Gagne, Y. C. Chiu, A. Chortos, F. Lissel, G. N. Wang, B. C. Schroeder, T. Kurosawa, J. Lopez, T. Katsumata, J. Xu, C. Zhu, X. Gu, W. G. Bae, Y. Kim, L. Jin, J. W. Chung, J. B. Tok, Z. Bao, Intrinsically Stretchable and Healable Semiconducting Polymer for Organic Transistors. *Nature* **2016**, *539*, 411.

[31] V. K. Sangwan, H. S. Lee, H. Bergeron, I. Balla, M. E. Beck, K. S. Chen, M. C. Hersam, Multi-Terminal Memtransistors from Polycrystalline Monolayer Molybdenum Disulfide. *Nature* **2018**, *554*, 500.

[32] H. Lee, S. Lee, Y. Kim, A. B. Siddik, M. M. Billah, J. Lee, J. Jang, Improvement of Stability and Performance of Amorphous Indium Gallium Zinc Oxide Thin Film Transistor by Zinc-Tin-Oxide Spray Coating. *IEEE Electron Device Lett.* **2020**, *41*, 1520.

[33] B. Jiang, Z. Yang, X. Liu, Y. Liu, L. Liao, Interface Engineering for Two-Dimensional Semiconductor Transistors. *Nano Today* **2019**, *25*, 122.

[34] Y. Wang, J. C. Kim, R. J. Wu, J. Martinez, X. Song, J. Yang, F. Zhao, A. Mkhoyan, H. Y. Jeong, M. Chhowalla, Van der Waals Contacts between Three-Dimensional Metals and Two-Dimensional Semiconductors. *Nature* **2019**, *568*, 70.

[35] P. Lin, F. Yan, Organic Thin-Film Transistors for Chemical and Biological Sensing. *Adv. Mater.* **2012**, *24*, 34.

[36] C. Qiu, Z. Zhang, M. Xiao, Y. Yang, D. Zhong, L.-M. Peng, Scaling Carbon Nanotube Complementary Transistors to 5-nm Gate Lengths. *Science* **2017**, *355*, 271.

[37] R. Hajian, S. Balderston, T. Tran, T. deBoer, J. Etienne, M. Sandhu, N. A. Wauford, J. Y. Chung, J. Nokes, M. Athaiya, J. Paredes, R. Peytavi, B. Goldsmith, N. Murthy, I. M. Conboy, K. Aran, Detection of Unamplified Target Genes via CRISPR-Cas9 Immobilized on A Graphene Field-Effect Transistor. *Nat. Biomed. Eng.* **2019**, *3*, 427.

[38] M. Ku, J. Kim, J.-E. Won, W. Kang, Y.-G. Park, J. Park, J.-H. Lee, J. Cheon, H. H. Lee, J.-U. Park, Smart, Soft Contact Lens for Wireless Immunosensing of Cortisol. *Sci. Adv.* **2020**, *6*, eabb2891.

[39] C. Dai, M. Guo, Y. Wu, B. P. Cao, X. Wang, Y. Wu, H. Kang, D. Kong, Z. Zhu, T. Ying, Y. Liu, D. Wei, Ultraprecise Antigen 10-in-1 Pool Testing by Multiantibodies Transistor Assay. *J. Am. Chem. Soc.* **2021**, *143*, 19794.

[40] C. Sun, R. Li, Y. Song, X. Jiang, C. Zhang, S. Cheng, W. Hu, Ultrasensitive and Reliable Organic Field-Effect Transistor-Based Biosensors in Early Liver Cancer Diagnosis. *Anal. Chem.* **2021**, *93*, 6188.

[41] D. Kong, X. Wang, C. Gu, M. Guo, Y. Wang, Z. Ai, S. Zhang, Y. Chen, W. Liu, Y. Wu, C. Dai, Q. Guo, D. Qu, Z. Zhu, Y. Xie, Y. Liu, D. Wei, Direct SARS-CoV-2 Nucleic Acid Detection by Y-Shaped DNA Dual-Probe Transistor Assay. *J. Am. Chem. Soc.* **2021**, *143*, 17004.

[42] A. Vacic, J. M. Criscione, N. K. Rajan, E. Stern, T. M. Fahmy, M. A. Reed, Determination of Molecular Configuration by Debye Length Modulation. *J. Am. Chem. Soc.* **2011**, *133*, 13886.

[43] N. Nakatsuka, K.-A. Yang, J. M. Abendroth, K. M. Cheung, X. Xu, H. Yang, C. Zhao, B. Zhu, Y. S. Rim, Y. Yang, P. S. Weiss, M. N. Stojanović, A. M. Andrews, Aptamer-Field-Effect Transistors Overcome Debye Length Limitations for Small-Molecule Sensing. *Science* **2018**, *362*, 319.

[44] D. T. Miyamoto, K. W. Mouw, F. Y. Feng, W. U. Shipley, J. A. Efstathiou, Molecular Biomarkers in Bladder Preservation Therapy for Muscle-Invasive Bladder Cancer. *The Lancet Oncol.* **2018**, *19*, e683.

[45] D. Margel, M. Pevsner-Fischer, J. Baniel, O. Yossepowitch, I. R. Cohen, Stress Proteins and Cytokines Are Urinary Biomarkers for Diagnosis and Staging of Bladder Cancer. *Eur. Urol.* **2011**, *59*, 113.

[46] S. L. Wood, M. A. Knowles, D. Thompson, P. J. Selby, R. E Banks,. Proteomic Studies of Urinary Biomarkers for Prostate, Bladder and Kidney Cancers. *Nat. Rev. Urol.* **2013**, *10*, 206.

[47] M. Frantzi, A. Latosinska, L. Fluhe, M. C. Hupe, E. Critselis, M. W. Kramer, A. S. Merseburger, H. Mischak, A. Vlahou, Developing Proteomic Biomarkers for Bladder Cancer: towards Clinical Application. *Nat. Rev. Urol.* **2015**, *12*, 317.

[48] M. Babjuk, M. Burger, E. M. Comperat, P. Gontero, A. H. Mostafid, J. Palou, B. W. G. van Rhijn, M. Roupret, S. F. Shariat, R. Sylvester, R. Zigeuner, O. Capoun, D. Cohen, J. L. D. Escrig, V. Hernandez, B. Peyronnet, T. Seisen, V. Soukup, European Association of Urology Guidelines on Non-muscle-invasive Bladder Cancer (TaT1 and Carcinoma In Situ) - 2019 Update. *Eur. Urol.* **2019**, *76*, 639.

[49] S. Bravaccini, V. Casadio, R. Gunelli, L. Bucchi, W. Zoli, D. Amadori, R. Silvestrini, D. Calistri, Combining Cytology, TRAP Cssay, and FISH Analysis for the Detection of Bladder Cancer in Symptomatic Patients. *Ann. Oncol.* **2011**, *22*, 2294.

[50] M. B. Amin, S. C. Smith, V. E. Reuter, J. I. Epstein, D. J. Grignon, D. E. Hansel, O. Lin, J. K. Mckenney, R. Montironi, G. P. Paner, H. A. Al-Ahmadie, F. Algaba, S. Ali, I. Alvarado-Cabrero, L. Bubendorf, L. Cheng, J. C. Cheville, G. Kristiansen, R. J. Cote, B. Delahunt, J. N. Eble, E. M. Genega, C. Gulmann, A. Hartmann, C. Langner, A. Lopez-Beltran, C. Magi-Galluzzi, J. Merce, G. J. Netto, E. Oliva, P. Rao, J. Y. Ro, J. R. Srihley, S. K. Tickoo, T. Tsuzuki, S. A. Umar, T. Van der Kwast, R. H. Young, M. S. Soloway, Update for the Practicing

Pathologist: The International Consultation on Urologic Disease-European Association of Urology Consultation on Bladder Cancer. *Modern Pathol.* **2015**, *28*, 612.

[51] B. Wang, C. Z. Zhao, Z. Q. Wang, K. A. Yang, X. B. Cheng, W. F. Liu, W. Z. Yu, S. Y. Lin, Y. C. Zhao, K. M. Cheung, H. S. Lin, H. Hojaiji, S. Emaminejad, Wearable Aptamer-Field-Effect Transistor Sensing System for Noninvasive Cortisol Monitoring. *Sci. Adv.* **2022**, *8*, eabk0967.

[52] Y. Zhao, Z. Wang, G. Xu, L. Cai, T. H. Han, A. Zhang, Q. Wu, R. Wang, T. Huang, P. Cheng, S. Y. Chang, D. Bao, Z. Zhao, M. Wang, Y. Huang, Y. Yang, High Performance Indium-Gallium-Zinc Oxide Thin Film Transistor via Interface Engineering. *Adv. Funct. Mater.* **2020**, *30*, 2003285.

[53] D. P. Kingma, J. Ba, Adam: A Method for Stochastic Optimization. *CoRR* **2015**, abs/1412.6980.

[54] F. Pedregosa, G. Varoquaux, A. Gramfort, V. Michel, B. Thirion, O. Grisel, M. Blondel, P. Prettenhofer, R. Weiss, V. Dubourg, J. Vanderplas, A. Passos, D. Cournapeau, M. Brucher, M. Perrot, E. Duchesnay, Scikit-learn: Machine Learning in Python. *J. Mach. Learn. Res.* **2011**, *12*, 2825.

A molecular specificity electronic device based on interface-engineered FET biosensor was engineered for noninvasive urinalysis. The urinalysis device achieves the reliable identification of five bladder tumor-associated proteins in urine samples. Integrating with a machine-learning algorithm, the device realizes a 95.0% bladder cancer diagnosis accuracy and could classify cancer stages with a 90.0% accuracy.

Yanbing Yang*, Jingfeng Wang, Wanting Huang, Guojia Wan, Miaomiao Xia, Duo Chen, Yun Zhang, Yiming Wang, Fuding Guo, Jie Tan, Huageng Liang, Bo Du, Lilei Yu*, Weihong Tan, Xiangfeng Duan, Quan Yuan*

Integrated Urinalysis Devices Based on Interface-Engineered Field Effect Transistor Biosensors Incorporated with Electronic Circuits